Experimental Evidence for the Formation of Solvation Shells by Soluble Species at a Non-Uniform Air – Ice Interface.

Thorsten Bartels-Rausch[+*], *Fabrizio Orlando*[+], *Xiangrui Kong*[+†], *Luca Artiglia*[+], *Markus Ammann*[+]

[+]Paul Scherrer Institut, Laboratory of Environmental Chemistry, CH-5232 Villigen PSI

Keywords: QLL, atmospheric chemistry, trace gas adsorption, XPS, NEXAFS

Abstract

Soluble species induce surface pre-melting at the air – ice interface in the thermodynamic ice stability domain below the liquidus. This quasi-liquid layer is thought to increase in thickness with concentration of impurities and to represent a reservoir into which larger amounts of soluble species dissolve compared to a more rigid ice surface. To directly investigate the response of the quasi-liquid layer to increasing amounts of solutes and to clarify the distribution of these at the ice surface with depth, we use a combination of Auger electron yield X-ray absorption and photoelectron spectroscopies. We studied the adsorption of formic acid to ice at 251 K. These two complimentary methods allow concluding that solutes enter the air – ice interface, but do not necessarily induce a thicker quasi-liquid layer. Rather, modifications of the hydrogen bonding

network seem to be linked to the formation of solvation shells and to long-range effects on the hydrogen-bonding network. We suggest that the flexibility of water molecules in the quasi-liquid layer is essential to form solvation shells and interpret the confinement of formic acid to the upper few ice bilayers to be linked with the structure of the hydrogen-bonding network getting more ice-like and rigid with depth at the air – ice interface.

TOC Graphic

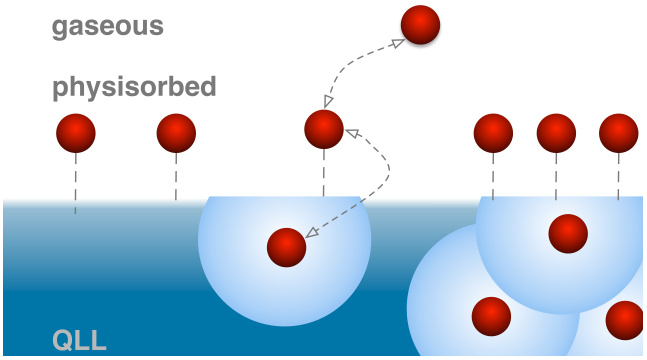

The pre-melting at the surface of ice crystals has been proposed to explain a number of large-scale environmental effects ranging from physical phenomena such as electrification of thunder clouds or the flow of glaciers[1] to chemical processes such as the scavenging of trace gases in ice clouds or the release of toxins[2]. This quasi-liquid at the edge of ice crystals, an example of the re-structuring found in any solid close to its melting point[3], has been extensively studied by theory, simulations, and diverse experimental techniques during the last decades, also because ice is seen as an excellent model system for phase transitions and interface phenomena in material science. Despite general agreement on the appearance of the quasi-liquid on ice when temperatures approach the melting point and on its enhancement in presence of impurities[4-8], the homogeneity and liquid-like character of the pre-melting layer remain controversial. Early optical reflection work by Elbaum et al.[8] suggested that in presence of impurities, the ice surface

is homogeneously wetted. The idea of a film spreading over the ice surface similar to a liquid has motivated describing the quasi-liquid in analogy to a homogeneous aqueous solution in chemical models used in environmental science[2]. However, molecular dynamics simulations indicate a more heterogeneous interface by suggesting that the presence of solutes leads to strongest modifications of the hydrogen-bonding network locally confined and in close neighbourhood to the impurity[2, 9-11].

We give direct experimental evidence of adsorbates entering the upper few nanometer of the air – ice interface accompanied by a restructuring of the hydrogen-bonding network. The findings using a combination of near ambient pressure X-ray photoelectron spectroscopy (XPS) and partial Auger electron yield near edge X-ray absorption fine structure (NEXAFS) spectroscopy suggest that the impurities engage water molecules in forming hydration shells rather than inducing a quasi-liquid layer. Probing the kinetic energy of photoemitted core electrons, XPS is one of the surface sensitive techniques with lowest detection limits and is element specific. Synchrotron-based XPS allows to obtain elemental ratios as a function of depth into the air – ice interface[12]. NEXAFS at the O K-edge directly reveals information about the arrangement of water molecules in the solid phase as well as in the liquid, as it directly probes electronic transitions to unoccupied states in the conduction band and is thus inherently sensitive to the water molecular orbital structure and subsequently to the H-bonding network[13]. Therefore, NEXAFS has been used to unravel the disorder in the hydrogen bonding network in presence of acids[12, 14].

We perform experiments on ice samples in thermodynamic equilibrium with gas phase water partial pressure[15]. During the experiments the response of the sample to increased gas-phase exposure to formic acid within the ice stability domain approaching the thermodynamic liquidus

phase boundary was investigated. Formic acid was chosen as probe molecule, because of its relevance in atmospheric and cryospheric science. Formic acid is one of the most abundant volatile organic acid and contributes significantly to acidification of precipitation[16]. In polar environments and the upper troposphere, where surface snow and ice clouds, respectively, are present, exchange of volatile organic compounds has been shown to be key in understanding geo-chemical cycles of pollutants and predicting the oxidative capacity of the atmosphere[17-18]. Gas-phase concentrations of formic acid in Greenland and at South Pole have been reported to roughly exceed 1 ppb (~10^{-6} mbar at atmospheric pressure) in the air filling the pore space of surface snow[19]. Further, formic acid has recently revoked interest as hydrogen storage material in environmental and energy research[20], and its interaction with frozen matter is of interest to astrophysics and –chemistry[21]. Besides these concrete factors, formic acid was also chosen to facilitate comparison with our previous work focusing on acetic acid[12]. Both organics are weak acids and share a similar solubility in water.

Experimental

Ice samples were exposed to formic acid at 0.01 mbar and 0.05 mbar in a flow-through cell at a constant partial pressure of water of 0.86 mbar, corresponding to the vapour pressure of ice at 251 K[22]. Pressure was measured by a capacity manometer (MKS Baratron 626A) with a measurement range from 5×10^{-4} to 1 mbar and an accuracy of 0.25 % of the reading. The ice was grown in-situ on a gold coated sample holder from water vapour at 250 K for 30 min. A partial pressure of 0.01 mbar (0.05 mbar) formic acid in the sample chamber was set via a quartz capillary from liquid formic acid (Sigma Aldrich #33015, p.a. ACS) that had been degassed by 3 freeze-pump-thaw cycles and was kept in a temperature controlled reservoir.

Two sets of XPS and NEXAFS measurements were done *en bloc*: 5 h – 8 h after dosing was started and 2 h – 4 h after the dosing was increased, respectively, giving the system ample time to establish adsorption equilibrium and a steady-state for bulk diffusion. The experiments were done at the SIM beamline of the Swiss Light Source (SLS) at the Paul Scherrer Institute using the Near Ambient Pressure Photoemission (NAPP) endstation described earlier[15].

The XPS work presented here follows a procedure established earlier[12] and aims at determining the ratio of C1s to O1s PE intensities to discuss concentrations of formic acid at the ice surface. To clearly identify changes in the C1s spectrum taken in presence of formic acid, 4 × C1s and 1 × O1s spectra were acquired alternating with a monochromatic incident X-ray beam at a photon energy of 735 eV. An average of 15 runs prior to and of 15 runs in presence of 0.01 mbar formic acid was used to derive spectra with sufficient signal to noise ratio. To quantify the concentration of formic acid at the air – ice interface and to derive depth profiles, it is essential that the C1s and O1s spectra probe the same depth in the sample. In XPS, as well as Auger yield NEXAFS spectroscopy, the volume from which the emitted electrons originate is a direct function of their kinetic energy. Here, we use the term mean electron escape depth (*ED*) to refer to the depth from which the integrated total number of electrons is emitted. The mean escape depth directly relates to the average distance that an electron with a given kinetic energy travels through the sample without experiencing inelastic collisions (inelastic mean free path, IMFP):

$$ED = IMFP \times \cos(\theta) \qquad (1)$$

where $\theta = 30°$ is the angle to the surface normal at which the electrons are detected by the analyser[15]. Thus, C1s and O1s PE spectra were acquired at the same kinetic energies of the emitted electrons of 150, 200, 240 395, 440, 540, 1060, 1300 eV using varying photon energies of the incident X-ray beam ranging from 440 eV to 1590 eV. Inevitably, the C1s and

corresponding O1s measurements were not performed at the same time. To confirm high data quality and exclude a trend in ice sample thickness affecting signal intensity, an increase of the O1s PE intensities with kinetic energy following the trend of electron escape depth was ensured and repeated measurements at fixed kinetic energy during the course of the beam time were performed.

XPS is a quantitative spectroscopic method and molecular mixing ratio of formic acid were derived as follows[12]: The C1s to O1s PE intensity ratio were calibrated ($I_{C1s(FA)}/I_{O1s}$) by recording C1s and O1s PE gas-phase spectra taken in presence of CO_2 with a partial pressure of 0.5 mbar in the sample chamber. The $I_{C1s(FA)}/I_{O1s}$ corresponds to the atomic ratio ($n_{C(FA)}/n_O$) accounting for variations in beamline flux at the sample spot, in absorption cross section, and in the electron analyser's transmission. Deviations in beamline settings during the calibration measurements were taken into account by using published electron absorption cross section data[23] and in-situ flux measurements at the refocusing mirror of the beamline. Given that only part of the oxygen is that of ice as formic acid also holds two oxygen atoms per molecule, the atomic ratio translates to a mole fraction using $n_{FA}/n_{ice} = \frac{n_{C(FA)}/n_O}{1-2\times n_{C(FA)}/n_O}$ to convert the atomic ratio into a molar mixing ratio (n_{FA}/n_{ice}) and $X_{FA} = \frac{n_{FA}/n_{ice}}{1+n_{FA}/n_{ice}}\times 100$ to compute the mole fraction of formic acid X_{FA}. For all of these XPS measurements, pass energy of the hemispherical electron energy analyser (Scienta R4000 HiPP-2) was set to 20 or 50 eV and dwell time to 0.1 s. The O1s and C1s spectra were fitted using the XPST front-end of IgorPro by symmetric Gaussian-Lorentzian functions using binding energy constrains, as discussed in the results section, and with equal peak width for all components of each PE spectrum.

X-ray absorption was measured at the oxygen K-edge by sweeping the X-ray photon energy in increments of 0.2 eV across 529 eV to 542 eV and of 0.5 eV over the remaining regions. A 450-470 eV kinetic energy window corresponding to the tail of the oxygen Auger region was used for detection. The NEXAFS spectra were normalized to background measurements (I_0) to account for variations in beamline flux with photon energy as derived from in-situ flux measurements at the refocusing mirror of the beamline; to drifts in the pre-edge region using a linear fit; and to their integrated area between 534 eV and 545 eV photon energy to facilitate comparison. Polarization of the incoming X-ray beam was set to 54.7° Dwell time and pass energy were set to 0.1 s and 20 eV, respectively. A NEXAFS measurement took about 30 min.

Results and Discussion

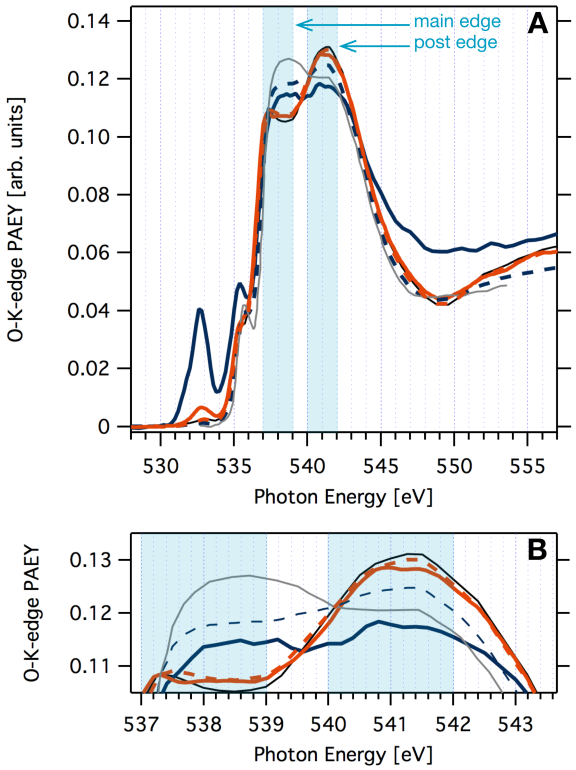

Figure 1. A Oxygen K-edge partial Auger electron yield X-ray absorption spectra of the ice sample at 251 K in presence of 0.01 mbar (orange solid line) and 0.05 mbar (navy solid line) partial pressure of formic acid. The dashed lines are representation of the experimental data based on linear combinations of the O K-edge NEXAFS spectra of neat ice at 251 K (black line) and of neat water at 269 K (grey line). The water NEXAFS was not acquired in this work[24]. **B** Zoom into the main and post edge region.

Figure 1 shows X-ray absorption spectra of ice at the oxygen K-edge in presence of formic acid at different gas-phase partial pressures. The spectra show distinct differences at 533 eV and in the spectral region between the main absorption edge at 537 eV and the post-edge centred at 541 eV. The peak in the NEXAFS spectrum at 533 eV is due to the contribution of oxygen in the carboxyl of formic acid and from carbonyl and carboxyl groups carbon contamination possibly present in the system prior to and during admission of formic acid (see later). The absorption in the main- and post-edge region of the NEXAFS spectra originates from oxygen in water molecules. At a formic acid partial pressure of 0.01 mbar, the spectrum of the sample (orange line) closely resembles that of neat crystalline ice (black line) which is characterized by an intense post-edge peak and a less pronounced main-edge peak. Upon increasing the partial pressure of formic acid to 0.05 mbar (navy blue line), the post-edge peak loses intensity relative to the main-edge peak, the shape of the NEXAFS spectrum seems to approach that of liquid water (grey line). Bluhm et al.[7] discussed a similar trend in O K-edge NEXAFS spectra of neat ice when temperature was increased from 234 K to 271 K showing that this technique can resolve such changes at the nanometer scale of the air – ice interface. Obviously, the NEXAFS spectrum at 0.01 mbar is dominated by features present in the spectrum of ice and at 0.05 mbar these features are still prominent.

Liquid-like Character of the Air – Ice Interface

We interpret the observed spectra to reflect different relative contributions from water molecules adopting a structure as in ice and water molecules coordinated as in solution. Then, we can conclude that even though a significant fraction of water molecules preserves its ice-like structure as given by the temperature of the experiment, the increase of formic acid density results in an overall increase of water molecules experiencing a liquid-like character of the hydrogen bonding network at the air – ice interface. The increase of the water-like features in the NEXAFS spectrum bears the question of crossing the liquidus and observing melting of the sample. To the best of our knowledge, the phase diagram of formic acid – water binaries is not known. Melting point depression data[25] and Henry's law coefficient based on thermodynamic calculations[26] and as used in earlier studies[27-28] indicate that the phase boundary at 251 K is crossed at 0.07 mbar. Based on more recent Henry's law coefficient measurements in milli-molar formic acid solutions[29], the liquidus is located at 0.02 mbar indicating a brine in thermodynamic equilibrium with ice in these experiments. Yet, apparent Henry's law coefficients of formic acid show a strong trend with concentration[30], justifying the use of the calculated Henry's law coefficient for the 10 molar formic acid solution in equilibrium with ice at 251 K[25]. Therefore, we conclude that our work was done in the ice stability domain. Support comes from optical inspection of the sample in-situ during the measurements using an endoscope camera showing no indication of macroscopic melting. Furthermore, potential loss of formic acid during gas-phase transport to the sample at the walls of the set-up, make it appear likely that the partial pressure of formic acid at the ice sample was substantially lower than measured upstream of the sample.

Interestingly, the observed NEXAFS spectrum in presence of low amounts of formic acid (solid orange line) shows excellent agreement with a linear combination (dashed orange line) of

the spectra of neat ice (90 %) and that of water (10 %). A linear combination (dashed navy blue line) based on 40 % of the spectrum of neat ice and 60 % of neat water represent the shape of the main- and post-edge in the NEXAFS spectrum at higher dosage of formic acid relatively well indicating that formic acid has the potential to induce changes in the hydrogen-bonding of a significant fraction of water molecules at the air – ice interface. In lack of a NEXAFS measurement of an aqueous formic acid solution at a concentration in equilibrium with the ice phase at 251 K, uncertainty in these quantitative estimates comes from the use of the bulk sensitive water NEXAFS recorded in transmission mode at 269 K[24]. The main- (post-) edge relative intensity has been observed to decrease (increase) in the temperature range of 299 K to 264 K in neat water samples[24]. While this temperature trend would render the difference between the NEXAFS spectra in presence of formic acid and of neat water smaller, solutes such as halides[31] or nitrate[14] have the opposite effect on the NEXAFS spectra.

Concentration and Hydrogen Bonding of Formic Acid

Given the importance of surface concentration in this discussion, we now turn to the interpretation of the photoemission spectra and the information on the concentration and depth distribution of formic acid at the air – ice interface that they reveal.

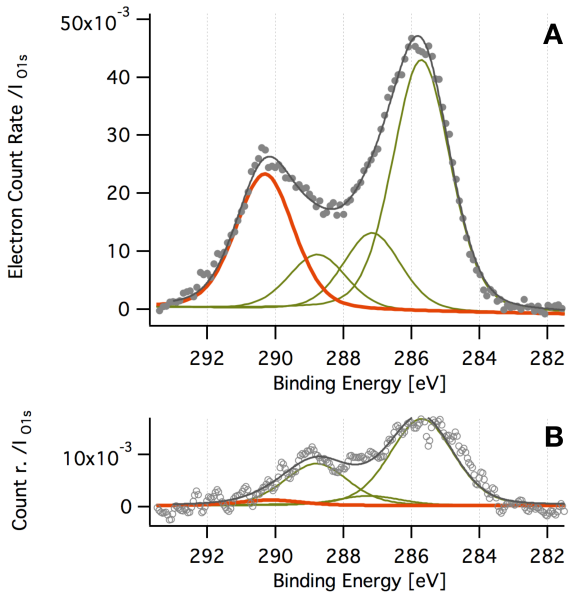

Figure 2. C1s photoelectron spectra relative to the intensity of oxygen from O1s photoelectron spectra of ice samples at 251 K at a partial pressure of 0.01 mbar formic acid (**A:** full circles) and prior to the exposure (**B:** open circles). The dark grey lines show results from fitting four Gaussian-Lorentzian peaks representing typical functional carbon groups of adventitious carbon (green lines) and the carboxylic group of formic acid (orange line) to the data. The measurements were done with a photon energy of 735 eV, the binding energies are referenced to the binding energy of the O1s peak of ice constrained at 533.2 eV[12].

Figure 2 shows the change in the C1s photoelectron spectrum upon exposure of the ice sample to 0.01 mbar formic acid partial pressure at 251 K. A distinct feature emerges at the high binding energy side of the spectrum in the presence of formic acid. This peak is centered at an electron binding energy (BE) of 289.5 eV which we attribute to neutral HCOOH. Both spectra further reveal broad features between 285 eV and 288 eV, which can be deconvoluted into a dominating peak at 284.9 eV and two minor components centered around 286.5 eV and 288 eV, respectively. For this, the fits were constrained to BE shifts of 1.45-1.55 eV, 3.0-3.15 eV, and 4.45-4.55

relative to the fourth, low BE feature. The BE of the fourth feature in the C1s PE spectrum prior to dosing was set to the same BE as found in the spectrum in presence of 0.01 mbar formic acid. These features are consistent with typical C-C, C-O, and C=O components found in adventitious carbon[32]. Adventitious carbon is formed from gaseous carbon-precursors via a cascade of radical reactions involving low energy secondary electrons. In presence of formic acid, the adventitious carbon increases significantly in intensity, in line with a higher partial pressure of organic precursors. Beam-damage of adsorbed formic acid might also contribute to the increase of these features. Note that formic acid seems particularly prone to form adventitious carbon; in presence of 0.1 mbar methanol no increase of adventitious carbon was observed on an ice sample at 253 K (not shown). Interestingly, the HCOOH feature at 289.5 eV is chemically shifted by 4.6 eV relative to the aliphatic feature of adventitious carbon. This larger shift compared to the 4.0 eV found in gas-phase carboxyl groups[33] is an important finding differentiating this peak from the less oxidized components of the adventitious carbon. The increase in binding energy indicates additional electron withdrawing binding partners of formic acid at the air – ice interface, that are absent in the gas phase. It might thus be explained by the formation of hydrogen bonds at the carboxyl oxygen of formic acid with the water molecules at the surface via adsorption, as previously argued for acetone adsorption to ice[34], and at the air – ice interface via formation of solvation shells. The more hydrophobic adventitious carbon, on the other hand, interacts with the ice surface via weaker van der Waals interactions.

From such a PE intensity ratio as shown in Figure 2, but at constant kinetic energy, direct quantitative information of the formic acid concentration can be derived after calibration (experimental part). Doing so and assuming, for comparison reasons, that the total number of formic acid molecules detected by XPS is adsorbed at the surface of ice, surface coverages of

3×10^{14} molecules per cm^2, which is in the range of saturated Langmuir monolayer[35], are found for the data at 0.01 mbar formic acid partial pressure. This apparent surface coverage is lower than predicted by extrapolating the temperature dependent Langmuir partitioning coefficient where, based on data between 190 K and 230 K, monolayer coverage is reached at lower partial pressure of formic acid of 1×10^{-3} mbar at 251 K[35]. Given that no adsorption isotherm data are available for the temperature of 251 K and that formic acid might be lost during transport to the sample, we refrain from a detailed comparison.

Water Availability in the Air – Ice Interface

Now that we have established the surface concentration of formic acid is not exceeding a monolayer when dosing 0.01 mbar in our experimental set-up, we can compare the findings to the situation of acetic acid[12] at 230-240 K. A marked difference is revealed by the NEXAFS measurements (Figure 1) showing a higher amount of water molecules adopting a liquid-like arrangement in presence of formic acid compared to the presence of acetic acid, for which even smaller changes to the NEXAFS spectra were observed at similar surface coverage[12]. Below 240 K, the varying ability of acetone, acetic acid, and nitric acid to engage water molecules in forming a liquid-like hydrogen bonding arrangement has been linked to the solubility in water at room temperature which differs by orders of magnitude[12]. Both organic acids have a similar solubility in water at low concentration with a Henry's law constant of 88 mol m^{-3} Pa^{-1} for formic acid and 40 mol m^{-3} Pa^{-1}[29] for acetic acid. A key difference in the two experiments was the temperature of the ice sample, and we therefore conclude that an enhanced availability of water seems to facilitate the shift towards the liquid-like character. Differences in water availability can be linked to the neat QLL where the water molecules are mobile enough to fulfil the hydration demand. We conclude that the neat QLL facilitates a shift in the sorption mechanism from

surface adsorption only to solvation featuring solvation shells at the air – ice interface. The abrupt appearance of solvation shells above 250 K is in line with a step-wise extension of the QLL into the uppermost bi-layer of the pure ice crystal at an on-set temperature of 257 K as shown in a recent vibrational sum-frequency generation spectroscopy study[36] and with earlier NEXAFS studies showing that the QLL starts to evolve between 248 K and 258 K[7].

Formic Acid Depth Profiles

Next, we use the distinct peak in the C1s PE signal at 289.5 eV to investigate the distribution of formic acid with depth at the ice – air interface. For this, the PE spectra of C1s and O1s were measured at varying photoelectron kinetic energies between 150-1300 eV. Given that the inelastic mean free path of electrons increases with energy in this photoelectron kinetic energy range, integrated C1s and O1s PE intensities probing volumes from the sample surface to increasing depths were obtained. Figure 3 shows the resulting $I_{C1s(FA)}/I_{O1s}$ ratio as a function of photoelectron kinetic energy for the two experiments shown in Figure 1. These depth profiles reveal distinct differences: The $I_{C1s(FA)}/I_{O1s}$ ratio shows a strong decrease over the whole photoelectron kinetic energy range at lower formic acid partial pressure and a significantly less pronounced decrease of the intensity ratio with photoelectron kinetic energy at higher formic acid partial pressure. With increasing photoelectron kinetic energy, the probed sample volume increases from the ice surface downwards. A species with homogeneous concentration along the entire depth of the air – ice interface would show steady increase of both $I_{C1s(FA)}$ and of I_{O1s} and consequently a constant $I_{C1s(FA)}/I_{O1s}$ in Figure 3. The other extreme, a species that is purely surface adsorbed would result in a constant $I_{C1s(FA)}$ regardless of the electron kinetic energy, an increase of I_{O1s} as the number of water molecules growths with probing volume, and thus a strongly decreasing $I_{C1s(FA)}/I_{O1s}$. Therefore, the steep profile of the integrated signal indicates

that the formic acid is predominantly located at the surface and its availability decreases strongly with depth, while the shallow profile indicates some presence of formic acid also deeper in the ice.

The second difference is the higher absolute PE intensities ratio at higher dosing, in line with a larger amount of formic acid scavenged at the air – ice interface with increased partial pressure. Combined, the present study gives clear experimental evidence that an increase of formic acid concentration at the air – ice interface leads to stronger perturbation of the hydrogen-bonding network going along with the species taken up being found deeper in the interface of the ice sample.

Non-Uniform Air – Ice Interface

To quantitatively evaluate the depth at which formic acid is found near the surface of the ice and its concentration, a two-layer model was used in Figure 3 as described earier[12]. In this model, the formic acid is constrained to a thin layer sitting on top of neat ice. Equation 2 relates the ratio of the total PE signals from the ice sample with the number of carbon atoms of formic acid ($n_{C(FA)}$) and of oxygen atoms (n_O) per unit volume in an upper layer with thickness d.

$$\frac{I_{C1s(FA)}(E_{kin})}{I_{O1s}(E_{kin})} = \frac{n_{C(FA)}/n_O \times [1-e^{-d/ED}]}{1+n_{C(FA)}/n_O \times e^{-d/ED}} \qquad (2)$$

The mean electron escape depth (*ED*) relates to the probing depth at the ice surface and bears some uncertainty. Figure 3 shows the *ED* as calculated and used in earlier studies for crystalline ice[12] (grey solid line, right scale) and as estimated based on XPS measurements[37-38] for liquid water (grey dotted line, right scale). While the *ED* for crystalline and in particular liquid water have intrinsic uncertainties, the main uncertainty for this work comes from the large change with phase change of up to 50 % difference in *ED*. Given that the present interpretation of the

NEXAFS spectra indicate up to 60 % of the water molecules at the ice surface that are engaged in a local environment similar to liquid water, these estimates might give reasonable boundaries to the *ED* in the disordered interface. In this work, the fits of the depth profiles and the resulting thicknesses of layer *d* were found invariable to the choice of *ED* parameterization.

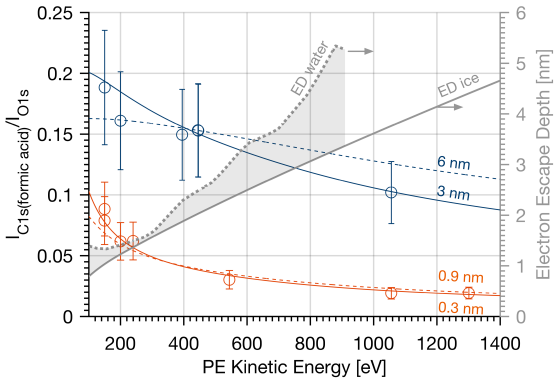

Figure 3. Ratio of the integrated PE intensities of the carboxylic peak area in C1s spectra and of the O1s peak area as a function of electron kinetic energy for experiments with 0.01 mbar (orange circles) and 0.05 mbar (navy blue circles) formic acid partial pressure. The error bars indicate the overall uncertainty. The colored lines represent fits to the data for different thicknesses of the sample fraction that homogeneously contain formic acid of 0.3 nm (solid orange line), 0.9 nm (dashed orange line), 3 nm (solid navy blue line), 6 nm (dashed navy blue line). The grey solid line (right scale) is the mean electron escape depth in ice versus electron kinetic energy based on calculated inelastic mean free path values for crystalline ice[39]. The grey dotted line gives the electron escape depth in water taken from recent measurements[37-38].

The decreasing $I_{C(FA)}/I_O$ with PE kinetic energy in Figure 3 are well reproduced with d = 0.3 - 0.9 nm (orange lines) for the case of 10 % water molecules engaged in a liquid-like hydrogen

bonding network. These fits to Eq. 2 return the variable $n_{C(FA)}/n_O$, the atomic ratio of carbon of formic acid to oxygen, which gives direct quantitative information of the formic acid concentration in *d*. With *d* = 0.3 nm (0.9 nm), we derive an atomic ratio of 0.37 (0.12) and an apparent surface coverage of 3×10^{14} molecules per cm^2 in full agreement with the direct estimate discussed above. Following Bluhm et al.[7], the NEXAFS measurements allow to derive the thickness of a liquid-like layer covering crystalline ice based on the signal attenuation by such an over-layer. With a maximal thickness of the QLL of 2-3 nm, as given by earlier NEXAFS work[7] and as discussed in the literature[2, 11], the 10 % disorder observed here would correspond to a liquid-like layer with a thickness of roughly one molecular ice layer. This estimate is in striking agreement to *d* from the depth profile (Figure 3) giving further support for formic acid entering the air – ice interface not significantly deeper than the first ice bilayer. A more detailed comparison is beyond the scope of this work. Given that the NEXAFS spectra in this work were recorded with a kinetic energy of the electrons of 430 – 450 eV, the signal intensity originates mostly from oxygen Auger electrons. However, also higher energy electrons with an initial kinetic energy of up to 530 eV might contribute to the signal as background via inelastic scattering. Thus, the ED of electrons could be slightly higher than based on the IMFP at 430 – 450 eV (Eq. 1). Nevertheless, the small *d* and the minor change in the NEXAFS point to the conclusion that, at an apparent monolayer coverage and 251 K, formic acid enters the ice within the depth of the neat-QLL and leads to some restructuring of the hydrogen-bonding network as compared to the QLL in absence of impurity. This spectroscopic difference is fully in line with sum frequency generation work showing substantial effects of solutes on the structure near the air – water interface[40].

Increasing the partial pressure of formic acid to 0.05 mbar, the data are reasonably well fitted with d = 3-6 nm indicating that the presence of formic acid is not restricted to the uppermost molecular bilayer in ice, but that formic acid resides within the upper few nm of the ice sample. The mole fraction of formic acid in the upper ice layers is 25 % with d = 3 and about 19 % with d = 6. This mole fraction is comparable to the mole fraction of a melt in equilibrium with ice at 251 K which is ~20 %[25]. At the same time, the NEXAFS (Figure 1) reveal that a significant fraction of water molecules in the sampling depth remain in an ice-like structure. Despite the remaining uncertainties in precisely quantifying the liquid-like fraction, this is clear evidence that the formic acid does not form a homogeneous liquid-like solution in the layer with thickness d, because we would then expect the NEXAFS to fully resemble that of the liquid. Rather, the data show that formic acid is found deeper in the ice than expected for a homogenous liquid-like layer. The liquid-like features as seen in the NEXAFS spectrum can then be explained by an interplay of water molecules hydrating the individual formic acid molecules in the ice forming solvation shells and the long-range effects of formic acid[41] and solutes in general[42] on the hydrogen-bonding network. Semantically, we would refer to d as the thickness of the QLL taken that the mixing ratio of formic acid in these upper ice layers is orders of magnitudes too high for solid solutions. Typical mole fractions of highly soluble gases, such as HCl or formaldehyde, in ice scale up to 1 x 10^{-5} [43-44]. Given that we work in the ice stability domain, the non-uniform character at the air – ice interface observed here is distinct from enhancement of solutes at the surface of frozen salt solutions as observed by Raman microscopy on the μm scale and that was explained by formation of brine micropockets[45].

Emerging Picture of the Air – Ice Interface

The emerging picture of the role of the QLL in gas sorption is that once the neat QLL evolves it satisfies the adsorbate's demand of water molecules for hydration. This is in line with observed changes of the Raman OH-stretch band at the ice surface upon adsorption of HCl and HNO_3 at 258 K by the Donaldson group[46]. At 230 K, a temperature where O K-edge NEXAFS do not indicate the presence of a QLL on neat ice[7], the Ammann group reported HNO_3 adsorption to significantly modify the structure of the hydrogen-bonding network [14] indicating that highly soluble, strong acids are capable to attract water molecules to form solvation shells even from more rigid surfaces as compared to the weaker formic and acetic acid. Increasing the load of acid at the air – ice interface, the additional demand of water molecules is satisfied by the solute entering deeper into the ice of the interface region. Our data show that the depth at which formic acid is found remains within a few nanometer during the course of the experiments of 2 h. This might indicate that the QLL gradually gets more rigid and ice-like with depth, in line with sum-frequency generation spectroscopy work indicating that the QLL is not homogeneous along the surface normal[47]. Obviously, then the depth into which formic acid enters the QLL is given by the energetics of the overall system as given by forming additional hydrogen bonds with water molecules in a more rigid structure deeper in the QLL. This situation, where the disorder increases upon approaching the border of the phase diagram is similar to results from pioneering ellipsometry work by the McNeill group for hydrochloric acid[6], nitric acid[5], formaldehyde, and acetaldehyde[4]. Accompanying flow-tube work showed that the nature of the interaction of gas-phase hydrochloric acid changed from an adsorptive one to a constant flux from the surface into the QLL[6]. The total number of molecules taken up by the ice remained similar in both regimes: Our data indicate a pronounced increase of the formic acid concentration in ice from a total of 3×10^{14} molecules cm^{-2} apparent surface coverage at low dosing to 2-3 x 10^{15} molecules cm^{-2}

only at higher dosing. Even more striking, this translates into bulk concentrations in the upper nanometers of the air – ice interface with mole fraction exceeding those in a saturated solid solution by orders of magnitude. Further, solvation in the QLL apparently goes along with substantial dissociation of acids[12, 48]. At the surface of the QLL, however, Kong, et al. [48] gave experimental evidence for the presence of molecular adsorbed HCl, supporting earlier spectroscopic work by the Donaldson group showing that the dissociation of HCl is hindered at the air – ice interface[49]. Disentangling the dissociation degree was beyond the scope of this work, but this Janus-type behavior of acids across interfaces certainly needs further attention.

Conclusion

While the environmental implication of the QLL to act as reservoir for formic acid at 251 K is limited as the pronounced uptake is only observed at higher gas-phase mixing ratio than found in Earth's atmosphere, this study links observations on the molecular scale to form an emerging picture of physical processes at the interface. This study identifies clear differences between the neat-QLL and the impurity induced-QLL and suggest that in presence of a QLL impurities tend to form solvation shells and thus establish a liquid-like environment in their close neighborhood. We further give experimental evidence that the QLL is not a uniform layer, but that its chemical properties change gradually with depth. Even though we probe this with high concentrations of formic acid, we believe that this is an inherent feature of the QLL independent of the dopant concentration. We propose that the liquid-like environment established in neighborhood of dopants might even impact key steps in chemical reactions, such as the photolysis cross sections. Generally, the air – ice interface with its high concentration of solvated solutes seems to be distinct from bulk ice, as well as from bulk solutions given that the hydrogen bonding network at the air – ice interface keeps a predominately ice-like character. Application of this *Janus*-type

character at the air – ice interface to models is not straight forward, as it is not *per se* clear for which type of chemical process the liquid-like or the ice-like character dominates. This emerging picture is thus essential for understanding chemistry in the cryosphere at temperatures close to the melting point and the liquid-like character of snow and ice with its wide geophysical implications in Earth's environment where impurities are omnipresent.

AUTHOR INFORMATION

Corresponding Author

*To whom correspondence should be addressed. Email: thorsten.bartels-rausch@psi.ch.

Present Addresses

† Nano and Molecular Systems research unit, University of Oulu, P.O. Box 3000, 90014 University of Oulu, Finland.

Author Contributions

The manuscript was written through contributions of all authors. All authors have given approval to the final version of the manuscript. TBR designed and supervised the research, analyzed the data, and wrote the manuscript. FO developed and supervised the X-ray spectroscopy. MA designed the research. FO, XK, LA, TBR performed the research.

Funding Sources

Swiss National Science Foundation (SNF) with grants #149629 and #169176. Swedish Research Council (#2014-6924).

ACKNOWLEDGMENT

We thank the staff of PSI/SLS for excellent beam quality and the beamline scientists at SIM for their support. The engineering work and technical support by Mario Birrer is greatly acknowledged. We thank Astrid Waldner for her continuous work on and contribution to this project. This work was supported by the Swiss National Science Foundation (SNF) with grant #149629. XK acknowledges funding from the Swedish Research Council (#2014-6924) and FO from SNF grant #169176.

REFERENCES

1. Dash, J. G.; Fu, H. Y.; Wettlaufer, J., The Premelting of Ice and Its Environmental Consequences. *Rep. Prog. Phys.* **1995,** *58* (1), 115-167.
2. Bartels-Rausch, T.; Jacobi, H.-W.; Kahan, T. F.; Thomas, J. L.; Thomson, E. S.; Abbatt, J. P. D.; Ammann, M.; Blackford, J. R.; Bluhm, H.; Boxe, C. S.; Dominé, F.; Frey, M. M.; Gladich, I.; Guzman, M. I.; Heger, D.; Huthwelker, T.; Klan, P.; Kuhs, W. F.; Kuo, M. H.; Maus, S.; Moussa, S. G.; McNeill, V. F.; Newberg, J. T.; Pettersson, J. B. C.; Roeselova, M.; Sodeau, J. R., A Review of Air–Ice Chemical and Physical Interactions (AICI): Liquids, Quasi-Liquids, and Solids in Snow. *Atmos. Chem. Phys.* **2014,** *14* (3), 1587-1633.
3. Henson, B. F.; Robinson, J. M., Dependence of Quasiliquid Thickness on the Liquid Activity: A Bulk Thermodynamic Theory of the Interface. *Phys. Rev. Lett.* **2004,** *92* (24).
4. Kuo, M. H.; Moussa, S. G.; McNeill, V. F., Surface Disordering and Film Formation on Ice Induced by Formaldehyde and Acetaldehyde. *J. Phys. Chem. C* **2014,** *118* (50), 29108-29116.
5. Moussa, S. G.; Kuo, M. H.; McNeill, V. F., Nitric Acid-Induced Surface Disordering on Ice. *Phys. Chem. Chem. Phys.* **2013,** *15* (26), 10989-10995.
6. McNeill, V. F.; Loerting, T.; Geiger, F. M.; Trout, B. L.; Molina, M. J., Hydrogen Chloride-Induced Surface Disordering on Ice. *Proc. Nat. Acad. Sci.* **2006,** *103* (25), 9422-9427.
7. Bluhm, H.; Ogletree, D. F.; Fadley, C. S.; Hussain, Z.; Salmeron, N., The Premelting of Ice Studied with Photoelectron Spectroscopy. *J. Phys.: Condens. Matter* **2002,** *14* (8), L227-L233.
8. Elbaum, M.; Lipson, S. G.; Dash, J. G., Optical Study of Surface Melting on Ice. *J. Cryst. Growth* **1993,** *129* (3-4), 491-505.
9. Carignano, M. A.; Shepson, P. B.; Szleifer, I., Ions at the Ice/Vapor Interface. *Chem. Phys. Lett.* **2007,** *436* (1-3), 99-103.

10. Bauerecker, S.; Ulbig, P.; Buch, V.; Vrbka, L.; Jungwirth, P., Monitoring Ice Nucleation in Pure and Salty Water Via High-Speed Imaging and Computer Simulations. *J. Phys. Chem. C* **2008,** *112* (20), 7631-7636.
11. Dominé, F.; Bock, J.; Voisin, D.; Donaldson, D. J., Can We Model Snow Photochemistry? Problems with the Current Approaches. *J. Phys. Chem. A* **2013,** *117* (23), 4733-4749.
12. Krepelova, A.; Bartels-Rausch, T.; Brown, M. A.; Bluhm, H.; Ammann, M., Adsorption of Acetic Acid on Ice Studied by Ambient-Pressure XPS and Partial-Electron-Yield NEXAFS Spectroscopy at 230–240 K. *J. Phys. Chem. A* **2013,** *117* (2), 401-409.
13. Nilsson, A.; Nordlund, D.; Waluyo, I.; Huang, N.; Ogasawara, H.; Kaya, S.; Bergmann, U.; Näslund, L. A.; Öström, H.; Wernet, P.; Andersson, K. J.; Schiros, T.; Pettersson, L. G. M., X-ray Absorption Spectroscopy and X-ray Raman Scattering of Water and Ice; an Experimental View. *J. Electron. Spectros. Relat. Phenomena* **2010,** *177* (2-3), 99-129.
14. Krepelova, A.; Newberg, J. T.; Huthwelker, T.; Bluhm, H.; Ammann, M., The Nature of Nitrate at the Ice Surface Studied by XPS and NEXAFS. *Phys. Chem. Chem. Phys.* **2010,** *12* (31), 8870-8880.
15. Orlando, F.; Waldner, A.; Bartels-Rausch, T.; Birrer, M.; Kato, S.; Lee, M.-T.; Proff, C.; Huthwelker, T.; Kleibert, A.; van Bokhoven, J. A.; Ammann, M., The Environmental Photochemistry of Oxide Surfaces and the Nature of Frozen Salt Solutions: A New in Situ XPS Approach. *Top. Catal.* **2016,** *59* (5-7), 591-604.
16. Millet, D. B.; Baasandorj, M.; Farmer, D. K.; Thornton, J. A.; Baumann, K.; Brophy, P.; Chaliyakunnel, S.; de Gouw, J. A.; Graus, M.; Hu, L.; Koss, A.; Lee, B. H.; Lopez-Hilfiker, F. D.; Neuman, J. A.; Paulot, F.; Peischl, J.; Pollack, I. B.; Ryerson, T. B.; Warneke, C.; Williams, B. J.; Xu, J., A Large and Ubiquitous Source of Atmospheric Formic Acid. *Atmos. Chem. Phys.* **2015,** *15* (11), 6283-6304.
17. McNeill, V. F.; Dominé, F.; Grannas, A. M.; Abbatt, J. P. D.; Ammann, M.; Ariya, P. A.; Bartels-Rausch, T.; Donaldson, D. J.; Guzman, M. I.; Heger, D.; Kahan, T. F.; Klan, P.; Masclin, S.; Toubin, C.; Voisin, D., Organics in Environmental Ices: Sources, Chemistry, and Impacts. *Atmos. Chem. Phys.* **2012,** *12* (20), 9653-9678.
18. Grannas, A. M.; Bogdal, C.; Hageman, K. J.; Halsall, C. J.; Harner, T.; Hung, H.; Kallenborn, R.; Klan, P.; Klanova, J.; Macdonald, R. W.; Meyer, T.; Wania, F., The Role of the Global Cryosphere in the Fate of Organic Contaminants. *Atmos. Chem. Phys.* **2013,** *13* (6), 3271-3305.
19. Dibb, J. E.; Arsenault, M., Shouldn't Snowpacks Be Sources of Monocarboxylic Acids? *Atmos. Environ.* **2002,** *36* (15-16), 2513-2522.
20. Mellmann, D.; Sponholz, P.; Junge, H.; Beller, M., Formic Acid as a Hydrogen Storage Material – Development of Homogeneous Catalysts for Selective Hydrogen Release. *Chem. Soc. Rev.* **2016,** *45* (14), 3954-3988.
21. Bennett, C. J.; Hama, T.; Kim, Y. S.; Kawasaki, M.; Kaiser, R. I., Laboratory Studies on the Formation of Formic Acid (HCOOH) in Interstellar and Cometary Ices. *Astrophys. J.* **2011,** *727* (1), 27.
22. Marti, J.; Mauersberger, K., A Survey and New Measurements of Ice Vapor Pressure at Temperatures between 170 and 250 K. *Geophys. Res. Lett.* **1993,** *20* (5), 363-366.
23. Yeh, J. J.; Lindau, I., Atomic Subshell Photoionization Cross-Sections and Asymmetry Parameters *Atomic Data and Nuclear Data Tables* **1985,** *32* (1), 1-155.

24. Sellberg, J. A.; Kaya, S.; Segtnan, V. H.; Chen, C.; Tyliszczak, T.; Ogasawara, H.; Nordlund, D.; Pettersson, L. G. M.; Nilsson, A., Comparison of X-ray Absorption Spectra between Water and Ice: New Ice Data with Low Pre-Edge Absorption Cross-Section. *J. Chem. Phys.* **2014,** *141* (3), 034507.
25. Timmermans, J., Physico-Chemical Constants of Binary Systems in Concentrated Solutions, Volume 4 - Systems with Inorganic + Organic or Inorganic Compounds (Excepting Metallic Derivatives). Knovel.
26. Sander, R., Compilation of Henry's Law Constants (Version 4.0) for Water as Solvent. *Atmos. Chem. Phys.* **2015,** *15* (8), 4399-4981.
27. Lelieveld, J.; Crutzen, P. J., The Role of Clouds in Tropospheric Photochemistry. *J. Atmos. Chem.* **1991,** *12* (3), 229-267.
28. Jacob, D. J., Chemistry of Oh in Remote Clouds and Its Role in the Production of Formic Acid and Peroxymonosulfate. *J. Geophys. Res.* **1986,** *91* (D9), 9807-9826.
29. Johnson, B. J.; Betterton, E. A.; Craig, D., Henry's Law Coefficients of Formic and Acetic Acids. *J. Atmos. Chem.* **1996,** *24* (2), 113-119.
30. Servant, J.; Kouadio, G.; Cros, B.; Delmas, R., Carboxylic Monoacids in the Air of Mayombe Forest (Congo): Role of the Forest as a Source or Sink. *J. Atmos. Chem.* **1991,** *12* (4), 367-380.
31. Cappa, C. D.; Smith, J. D.; Wilson, K. R.; Messer, B. M.; Gilles, M. K.; Ronald C Cohen, a.; Saykally, R. J., Effects of Alkali Metal Halide Salts on the Hydrogen Bond Network of Liquid Water. *J. Phys. Chem. B* **2005,** *109* (15), 7046-7052.
32. Barr, T. L.; Seal, S., Nature of the Use of Adventitious Carbon as a Binding Energy Standard. *J. Vac. Sci. Technol., A* **1998,** *13* (3), 1239-1246.
33. Ratner, B. D.; Castner, D. G., Electron Spectroscopy for Chemical Analysis. Vickerman, J. C.; Gilmore, I. S., Eds. John Wiley & Sons, Ltd: Chichester, UK, 2009; pp 47-112.
34. Starr, D. E.; Pan, D.; Newberg, J. T.; Ammann, M.; Wang, E. G.; Michaelides, A.; Bluhm, H., Acetone Adsorption on Ice Investigated by X-ray Spectroscopy and Density Functional Theory. *Phys. Chem. Chem. Phys.* **2011,** *13* (44), 19988-19996.
35. von Hessberg, P.; Pouvesle, N.; Winkler, A. K.; Schuster, G.; Crowley, J. N., Interaction of Formic and Acetic Acid with Ice Surfaces between 187 and 227 K. Investigation of Single Species- and Competitive Adsorption. *Phys. Chem. Chem. Phys.* **2008,** *10* (17), 2345-2355.
36. Sánchez, M. A.; Kling, T.; Ishiyama, T.; van Zadel, M.-J.; Bisson, P. J.; Mezger, M.; Jochum, M. N.; Cyran, J. D.; Smit, W. J.; Bakker, H. J.; Shultz, M. J.; Morita, A.; Donadio, D.; Nagata, Y.; Bonn, M.; Backus, E. H. G., Experimental and Theoretical Evidence for Bilayer-by-Bilayer Surface Melting of Crystalline Ice. *Proc. Nat. Acad. Sci.* **2017,** *114* (2), 227-232.
37. Thürmer, S.; Seidel, R.; Faubel, M.; Eberhardt, W.; Hemminger, J. C.; Bradforth, S. E.; Winter, B., Photoelectron Angular Distributions from Liquid Water: Effects of Electron Scattering. *Phys. Rev. Lett.* **2013,** *111* (17), 173005.
38. Ottosson, N.; Faubel, M.; Bradforth, S. E.; Jungwirth, P.; Winter, B., Photoelectron Spectroscopy of Liquid Water and Aqueous Solution: Electron Effective Attenuation Lengths and Emission-Angle Anisotropy. *J. Electron. Spectros. Relat. Phenomena* **2010,** *177* (2-3), 60-70.
39. NIST Chemistry Webbook, NIST Standard Reference Database Number 69. Linstrom, P. J.; Mallard, W. G., Eds. National Institute of Standards and Technology, Gaithersburg MD, 20899, (accessed January 2013).

40. Jubb, A. M.; Hua, W.; Allen, H. C., Organization of Water and Atmospherically Relevant Ions and Solutes: Vibrational Sum Frequency Spectroscopy at the Vapor/Liquid and Liquid/Solid Interfaces. *Acc. Chem. Res.* **2012,** *45* (1), 110-119.
41. Aloisio, S.; Hintze, P. E.; Vaida, V., The Hydration of Formic Acid. *J. Phys. Chem. A* **2002,** *106* (2), 363-370.
42. Irudayam, S. J.; Henchman, R. H., Long-Range Hydrogen-Bond Structure in Aqueous Solutions and the Vapor-Water Interface. *J. Chem. Phys.* **2012,** *137* (3), 034508.
43. Thibert, E.; Dominé, F., Thermodynamics and Kinetics of the Solid Solution of HCl in Ice. *J. Phys. Chem. B* **1997,** *101* (18), 3554-3565.
44. Barret, M.; Houdier, S.; Dominé, F., Thermodynamics of the Formaldehyde–Water and Formaldehyde–Ice Systems for Atmospheric Applications. *J. Phys. Chem. A* **2011,** *115* (3), 307-317.
45. Morenz, K. J.; Donaldson, D. J., Chemical Morphology of Frozen Mixed Nitrate–Salt Solutions. *J. Phys. Chem. A* **2017,** *121* (10), 2166-2171.
46. Kahan, T. F.; Reid, J. P.; Donaldson, D. J., Spectroscopic Probes of the Quasi-Liquid Layer on Ice. *J. Phys. Chem. A* **2007,** *111* (43), 11006-11012.
47. Wei, X.; Miranda, P. B.; Shen, Y. R., Surface Vibrational Spectroscopic Study of Surface Melting of Ice. *Phys. Rev. Lett.* **2001,** *86* (8), 1554-1557.
48. Kong, X.; Waldner, A.; Orlando, F.; Artiglia, L.; Huthwelker, T.; Ammann, M.; Bartels-Rausch, T., Coexistence of Physisorbed and Solvated HCl at Warm Ice Surfaces. *J. Phys. Chem. Lett.* **2017**, 4757-4762.
49. Wren, S. N.; Donaldson, D. J., Laboratory Study of pH at the Air-Ice Interface. *J. Phys. Chem. C* **2012,** *116* (18), 10171-10180.